Math. Model. Nat. Phenom. 18 (2023) 29
https://doi.org/10.1051/mmnp/2023027

Mathematical Modelling of Natural Phenomena
www.mmnp-journal.org

AN ANALYSIS OF THE BUOYANCY AND DRAG PARAMETERS IN RAYLEIGH–TAYLOR DYNAMICS

Des Hill and Snezhana Abarzhi*

Abstract. Rayleigh–Taylor instability (RTI) is of critical important in a broad range of natural and industrial processes and is an intellectual challenge for theoretical studies. In this work, we analyze the scale-dependent linear and nonlinear Rayleigh–Taylor (RT) dynamics within the group theory approach. We link the governing equations, through an associated dynamical system based on space groups, to a momentum model based on scaling transformations. In doing so, we precisely derive expressions for the buoyancy and drag parameters of the momentum model, exactly integrate the model equations and determine solutions for bubbles and for spikes in both early-time and late-time regimes. In particular, we focus on the general situation in which the instability is driven by an acceleration having power-law time dependence. Our analysis provides extensive benchmarks for future research.

Mathematics Subject Classification. 76E17, 35Q35, 35Q85.

Received April 6, 2023. Accepted July 29, 2023.

1. Introduction

Rayleigh–Taylor instability (RTI) occurs whenever fluids of different densities are accelerated against their density gradient and leads to intense interfacial Rayleigh–Taylor (RT) mixing of the fluids [16, 26, 32]. This phenomenon plays an important role in many processes. Examples are supernovae, inertial confinement fusion, material deformation, and in the fossil fuel industry [3, 13, 14, 20, 38]. RT flows, whilst occurring in distinct physical circumstances, have similar evolution features [3, 5, 12, 16, 26, 29, 30, 34]. In realistic environments RTI are often driven by variable accelerations; it can be, for instance, a power-law function of time. Such accelerations can lead to new scaling properties and can be used to tune experiments in order to better fit observations.

RT dynamics is challenging to study as it requires one to solve the set of conservation laws - a system of nonlinear partial differential equations in four-dimensional space-time - subject to the nonlinear boundary value problem at the unstable interface and the ill-posed initial value problem. [5, 15, 19, 25, 26, 26, 37].

RTI stars to develop when the flow fields and/or the interface are slightly perturbed from their equilibrium state [16, 31]. The amplitude of the interface perturbation grows quickly. The RT unstable interface is composed of a large-scale coherent structure and small-scale irregular structures [12]. At large scales, bubbles of the lighter fluid move up into the heavier fluid and simultaneously spikes of the heavier fluid move down into the lighter fluid. Intense interfacial fluid movement ensues [5, 12, 19, 25, 30, 34, 37]. The respective velocity field in the bulk of each fluid is potential, and small-scale vortical structures at the interafce are driven by the interfacial shear.

Keywords and phrases: Rayleigh–Taylor instability, coherent structures, interfacial dynamics, variable acceleration.

University of Western Australia, Perth, WA 6009, Australia

* Corresponding author: snezhana.abarzhi@gmail.com

A group theory approach has proved to be very successful in advancing our understanding of RT dynamics, particularly in studying the interfacial and multi-scale character of RTI [3, 5, 12, 19, 25, 29, 30, 34, 37]. Here we apply this group theory approach [9, 21, 23] to precisely derive from the governing equations expressions for associated buoyancy and drag parameters of the momentum model for both early-time and later time RT dynamics driven by a time-varying acceleration. We exactly integrate the equations and find solutions for bubbles and for spikes in the early-time and the late-time regimes. Our results provide extensive benchmarks for future research.

We consider RTI in a 3D spatially extended periodic flow and apply group theory to solve the relevant boundary value problem, which involves boundary conditions at the interface and at the outside boundaries [1, 3, 7, 9]. We also solve the relevant momentum model of this flow, and, in doing so, obtain a number of important results. In particular, for both bubbles and spikes we find the family of nonlinear solutions, and identify a number of special solutions. These are being the critical, convergence-limit, Taylor, Layzer-drag and Atwood solutions. In each case we give the values of the curvature and velocity, along with corresponding buoyancy and drag coefficients.

The paper is organised as follows. In Section 2, the equations governing RTI are introduced, structural aspects of the instability are discussed and a pertinent dynamical system is derived using a group theory approach. The equivalent momentum model is then introduced, along with the times scales of the problem. Then follows an analysis of the defining equations. In Section 3, we present results for both the early-time and later time regimes. In addition, we discuss the special solutions mentioned in the previous paragraph. A summary and further discussion are given in the last section.

2. Description of the system

2.1. The governing equations

We consider immiscible, inviscid fluids of differing densities, separated by a well-defined interface. The heavier fluid sits above the lighter fluid and the entire system is subject to a time-dependent downwards acceleration field due to a body force. The dynamics of such fluids in governed by conservation of mass, momentum and energy:

$$\frac{\partial \rho}{\partial t}+\frac{\partial}{\partial x_i}(\rho v_i)=0, \qquad \frac{\partial}{\partial t}(\rho v_j)+\frac{\partial}{\partial x_i}(\rho v_i v_j)+\frac{\partial P}{\partial x_j}=0, \qquad \frac{\partial E}{\partial t}+\frac{\partial}{\partial x_i}((E+P)v_i)=0, \tag{2.1}$$

where $i,j=1,2,3$ and $(x_1,x_2,x_3)=(x,y,z)$ are the spatial coordinates, t is time, $(\rho,\mathbf{v},P,E)$ are the fields of density ρ, velocity $\mathbf{v}$, pressure P and energy density $E=\rho(e+\mathbf{v}\cdot\mathbf{v}/2)$, where e is the specific internal energy. An equation of state relates the pressure and specific internal energy, and for ideal fluids the ratio $P/(\rho e)$ is constant [3, 5, 8, 9, 26].

It is required that momentum must be conserved at the interface and that there can be no mass flux across it. Hence the boundary conditions at the interface are

$$\left[\rho\left(\frac{\dot\theta}{|\nabla\theta|}+\mathbf{v}\cdot\mathbf{n}\right)\right], \qquad [\mathbf{v}\cdot\mathbf{n}]=0, \qquad [P]=0, \qquad [\mathbf{v}\cdot\boldsymbol{\tau}]=\text{arbitrary}, \qquad [W]=\text{arbitrary}, \tag{2.2}$$

where $[\cdots]$ denotes the jump of functions across the interface; $\mathbf{n}$ and $\boldsymbol{\tau}$ are the normal and tangential unit vectors of the interface with $\mathbf{n}=\boldsymbol{\nabla}\theta/|\boldsymbol{\nabla}\theta|$ and $\mathbf{n}\cdot\boldsymbol{\tau}=0$; $\theta=\theta(x,y,z,t)$ is a local scalar function, with $\theta=0$ at the interface and $\theta>0$ ($\theta<0$) in the bulk of the heavy (light) fluid, indicated hereafter by subscript $h(l)$; $W=e+P/\rho$ is the specific enthalpy.

The initial conditions consist of initial perturbations of the flow fields in the fluid bulks and/or at the interface. The flow is periodic in the plane (x,y) normal to the z-direction. The acceleration is directed from the heavy to the light fluid and is the power-law function of time $g=Gt^a$ where $\mathbf{g}=(0,0,-g)$. Here a is the

acceleration exponent and $G > 0$ is the acceleration pre-factor and the acceleration strength. Their dimensions are $[G] = ms^{-(a+2)}$ and $[a] = 1$. This acceleration modifies the pressure field: $P \to P + \rho g z$. We assume that there are no mass sources and hence the velocity in the upper (lower) fluid vanishes far away from the interface $z \to \infty$ ($z \to -\infty$) as:

$$\mathbf{v}|_{\mathbf{z}\to+\infty} = 0, \qquad \mathbf{v}|_{\mathbf{z}\to-\infty} = 0. \tag{2.3}$$

2.2. Large-scale coherent structures

The large-scale coherent structures are arrays of bubbles and spikes periodic in the plane normal to the acceleration direction. The initial conditions determine the length and time scales of the problem. The length scale is set by the wave-vector k, and it is $1/k$, a multiple of the spatial period of the array, *i.e.*, the wavelength λ; the multiple depending on the symmetry type of the periodic structure. As a specific example, we consider the flow which has square symmetry [7, 9], in which case the wave-vector is $k = 2\pi/\lambda$.

The group theory approach [1, 3, 5, 7, 9] accurately describes the dynamics of the unstable interface and identifies similarities and differences in the dynamics of these flows. In particularly, for RTI with constant and time-varying accelerations and for Richtmyer–Meshkov (RM) instabilities with impulsive and time-varying accelerations, there are families of solutions in the nonlinear regime, with the number of relevant parameters defined by the flow symmetry; the dynamics is multi-scale and is characterised by the contributions of two macroscopic length scales, these being the spatial period and the amplitude of the coherent structure. Furthermore, the non-equilibrium dynamics is essentially interfacial, with intense motion of the fluids near the interface and effectively no motion away from the interface.

Even for ideal incompressible fluids, with $\dot{e} = 0$ and $\nabla e = 0$, the theoretical problem (2.1,2.2) is extremely challenging. One has to solve a system of nonlinear partial differential equations in four-dimensional space-time at the nonlinear freely evolving interface and also solve the relevant ill-posed initial value problem [3, 5, 9, 26]. Even with this amount of complexity, the dynamics nevertheless has remarkable features of universality and order and can thus be approached using group theory [3, 5]. Here, we implement the group theory approach and compare the principal resulting equation with the momentum model, the equations of which have the same symmetries and scaling transformations as the conservation laws [4–6, 8, 12].

2.3. The scales of the problem

We consider the dynamics in equations (2.1)–(3.2) in dimensional form, which requires us to identify the length-scale and the time-scale of the problem. The length scale of the problem is the wavelength λ, with corresponding wavenumber k.

The conditions at initial time t_0 are the initial curvature $\zeta(t_0)$ and the initial velocity $v(t_0)$. For a given wavelength λ and for $a \neq -2$, there are two natural time scales in the problem [24]. These are $\tau_g = (kG)^{-1/(a+2)}$ and $\tau_0 = 1/(kv_0)$ where $v_0 = |v(t_0)|$.

For $a < -2$, $\tau_0 \ll \tau_G$ and hence τ_0 is the smallest time scale, corresponding to the fastest process. This is the case in Richtmyer–Meshkov dynamics, which are driven by the initial growth-rate, and the relevant timescale is τ_0, see reference [24]. For $a > -2$, $\tau_g \ll \tau_0$ and the dynamics is driven by the acceleration and the relevant time scale is τ_g. We refer to this as Rayleigh–Taylor (RT) dynamics. The transition case $a = -2$ has time scale $\tau_0 = 1/(kv_0)$ and the acceleration strength is parameterised by kG.

3. Methodology

3.1. The dynamical system

We focus on bubbles and spikes propagating in the z-direction and for convenience our calculations are performed in the frame of reference moving with velocity $v(t)$ in the z-direction, where $v(t) = \partial\eta_0/\partial t$ and $\eta_0(t)$ are the velocity and position of the bubble or spike in the laboratory reference frame. The interface function is $\theta(x, y, z, t) = z - \eta(x, y, t)$.

We consider incompressible dynamics with negligible effects of stratification and density variations, and focus on the large-scale coherent dynamics with length scale λ, presuming that the length scale of shear-driven interfacial vortical structures is small, $\ll \lambda$. The fluid motions are potential in the bulk and the velocity of the heavy (light) fluid is $\mathbf{v}_{h(l)} = \boldsymbol{\nabla}\Phi_{h(l)}$. For incompressible ideal fluids the equation for the conservation of mass leads to the Laplace equation $\nabla^2\Phi_{h(l)} = 0$ in the upper fluid bulk $z > \eta$ and the lower fluid bulk $z < \eta$.

The boundary conditions at the interface are

$$\rho_h\left(-\frac{\partial\eta}{\partial t} - \frac{\partial\eta}{\partial x}\frac{\partial\Phi_h}{\partial x} - \frac{\partial\eta}{\partial y}\frac{\partial\Phi_h}{\partial y} + \frac{\partial\Phi_h}{\partial z}\right) = 0, \qquad \rho_l\left(-\frac{\partial\eta}{\partial t} - \frac{\partial\eta}{\partial x}\frac{\partial\Phi_l}{\partial x} - \frac{\partial\eta}{\partial y}\frac{\partial\Phi_l}{\partial y} + \frac{\partial\Phi_l}{\partial z}\right) = 0,$$

$$\rho_h\left(\frac{\partial\Phi_h}{\partial t} + \frac{|\boldsymbol{\nabla}\Phi_h|^2}{2} + \left[g(t) + \frac{\mathrm{d}v}{\mathrm{d}t}\right]z\right) - \rho_l\left(\frac{\partial\Phi_l}{\partial t} + \frac{|\boldsymbol{\nabla}\Phi_l|^2}{2} + \left[g(t) + \frac{\mathrm{d}v}{\mathrm{d}t}\right]z\right) = f_B(t), \qquad z = \eta(x,y,t), \tag{3.1}$$

where $f_B(t)$ is arbitrary, and the vertical far-field boundary conditions are

$$\left.\frac{\partial\Phi_h}{\partial z}\right|_{z\to\infty} = -v(t), \qquad \left.\frac{\partial\Phi_l}{\partial z}\right|_{z\to-\infty} = -v(t). \tag{3.2}$$

The periodic nature of the large-scale coherent structure can be accommodated using group theory [5]. We first identify groups enabling structurally stable dynamics. The relevant symmetry group dictates a specific Fourier series (an irreducible representation of the group) which can be used to solve the nonlinear boundary value problem (3.1), (3.2). For three-dimensional flow with square symmetry $p4mm$ the potentials are [2, 7]

$$\Phi_h(x,y,z,t) = \sum_{m,n=0}^{\infty}\Phi_{mn}(t)\left(\frac{\cos(mkx)\cos(nky)\mathrm{e}^{-\alpha_{mn}kz}}{\alpha_{mn}k} + z\right) + f_h(t),$$

$$\Phi_l(x,y,z,t) = \sum_{m,n=0}^{\infty}\widetilde{\Phi}_{mn}\left(\frac{\cos(mkx)\cos(nky)\mathrm{e}^{\alpha_{mn}kz}}{\alpha_{mn}k} - z\right) + f_l(t), \tag{3.3}$$

where $\alpha_{mn} = \sqrt{m^2+n^2}$, m and n are integers, $k = 2\pi/\lambda$ is the wavenumber, Φ_{mn} and $\widetilde{\Phi}_{mn}$ are the Fourier amplitudes for the heavy and light fluids respectively, with $\Phi_{00} \equiv 0$, $\widetilde{\Phi}_{00} \equiv 0$, and $f_h(t)$ and $f_l(t)$ are time-dependent functions. Symmetry requires that $\Phi_{mn} = \Phi_{nm}$ and $\widetilde{\Phi}_{mn} = \widetilde{\Phi}_{nm}$.

We next make spatial expansions in the vicinity of the tip of the bubble or spike, as dictated by the relevant group. In this way, we reduce the governing equations to a system of ordinary differential equations in terms of interface variables and Fourier moments [1, 3, 5, 7, 9, 12].

In order to examine the local behaviour of the interfacial dynamics in the vicinity of the tip, we expand the interface function in a power series about $(x,y) = (0,0)$. In the moving frame of reference, this is

$$\eta(x,y,t) = \sum_{N=1}^{\infty}\sum_{i+j=1}^{N}\zeta_{ij}(t)x^{2i}y^{2j}, \tag{3.4}$$

where $\zeta_{ij}(t) = \zeta_{ji}(t)$ by symmetry, $\zeta(t) = \zeta_{10}(t) = \zeta_{01}(t)$ is the principal curvature at the tip and $N = i + j$ is the order of the approximation. The Fourier series and interface functions are substituted into the boundary conditions and the resulting expressions expanded in Taylor series. This yields an infinite system of ordinary

differential equations for the $\Phi_{mn}(t)$, $\widetilde{\Phi}_{mn}(t)$ and $\zeta_{ij}(t)$. We introduce the following moments of the heavy and light fluids, respectively:

$$M_{a,b,c}(t) = \sum_{m,n=0}^{\infty} \Phi_{mn}(t)(mk)^a(nk)^b(\alpha_{mn}k)^c, \qquad \widetilde{M}_{a,b,c}(t) = \sum_{m,n=0}^{\infty} \widetilde{\Phi}_{mn}(t)(mk)^a(nk)^b(\alpha_{mn}k)^c, \tag{3.5}$$

where m and n are non-negative integers. We note that by symmetry, $M_{a,b,c} = M_{b,a,c}$ and $M_{a+2,b,c} + M_{a,b+2,c} = M_{a,b,c+2}$ and similarly for $\widetilde{M}$. The moments are the weighted sum of the (infinite number of) Fourier amplitudes, and are the relevant correlation functions by their definitions. This representation in terms of moments M and $\widetilde{M}$, and the interface variables ζ accommodates the nonlocal nature of the nonlinear dynamics and enables us to investigate the interplay of harmonics.

To lowest order (that is, $N = 1$), the interface is $\eta(x, y, t) = \zeta(t)(x^2 + y^2)$. Note that $\zeta(t) < 0$, $v(t) > 0$ for bubbles, whereas for spikes $\zeta(t) > 0$, $v(t) < 0$. We abbreviate the series to second order in x and y, and to first order in z since $\eta(x, y, t)$ is quadratic in x and y. The boundary conditions at the interface become

$$\rho_h \left(\frac{\mathrm{d}\zeta}{\mathrm{d}t} - 4M_1\zeta - \frac{1}{2}M_2 \right) = 0, \qquad \rho_l \left(\frac{\mathrm{d}\zeta}{\mathrm{d}t} - 4\widetilde{M}_1\zeta + \frac{1}{2}\widetilde{M}_2 \right) = 0, \tag{3.6}$$

$$(1 + A) \left(\frac{1}{2}\frac{\mathrm{d}M_1}{\mathrm{d}t} + \zeta\frac{\mathrm{d}M_0}{\mathrm{d}t} - \frac{1}{2}M_1^2 - \zeta g \right) = (1 - A) \left(\frac{1}{2}\frac{\mathrm{d}\tilde{M}_1}{\mathrm{d}t} - \zeta\frac{\mathrm{d}\tilde{M}_0}{\mathrm{d}t} - \frac{1}{2}\widetilde{M}_1^2 - \zeta g \right), \tag{3.7}$$

$$\widetilde{M}_1 - M_1 = \text{arbitrary}, \tag{3.8}$$

and the vertical far-field requirements become

$$M_0 = -v(t), \qquad \widetilde{M}_0 = v(t), \tag{3.9}$$

where $M_0 = M_{0,0,0}$, $M_1 = M_{2,0,-1}$, $M_2 = M_{2,0,0}$ and the ratio of the fluid densities is parametrised by the Atwood number $A = (\rho_h - \rho_l)/(\rho_h + \rho_l)$.

3.2. The momentum model

The momentum model [4–6, 8, 9, 12] has the same symmetries and scaling transformations as the conservation laws, and balances, per unit mass, the rates of gain and loss of specific momentum, and in doing so, identifies invariant, scaling and spectral properties of the dynamics.

The dynamics of a parcel of fluid is governed by the balance per unit mass of the rate of momentum gain μ and the rate of momentum loss $\widetilde{\mu}$, as

$$\frac{\mathrm{d}h}{\mathrm{d}t} = v, \qquad \frac{\mathrm{d}v}{\mathrm{d}t} = \widetilde{\mu} - \mu, \tag{3.10}$$

where h is the displacement along the acceleration direction $\mathbf{g}$, v is the corresponding velocity, $\widetilde{\mu}$ and μ are the rates of gain and loss of specific momentum in that direction [4–6, 9, 12, 31, 35]. These rates are associated with the rates of gain $\widetilde{\epsilon}$ and loss ϵ of specific energy, as $\widetilde{\mu} = \widetilde{\epsilon}/v$ and $\mu = \epsilon/v$. The rate of gain of specific energy is $\widetilde{\epsilon} = Bgv$, where $g = |\mathbf{g}|$ and B is a buoyancy parameter. The rate of loss of specific energy is $\epsilon = Cv^3/L$ where L is the relevant length scale and C is a drag parameter. The quantities B and C are the parameters of the momentum model. They can be distinct in the scale-dependent linear and nonlinear regimes and in the

scale-invariant mixing regime. They can also be distinct for bubbles and for spikes. The length scale can be the horizontal scale (wavelength) $L \sim \lambda \sim k^{-1}$, or the vertical scale (amplitude) $L \sim |h|$. The cases $L \sim \lambda$ and $L \sim |h|$ correspond to scale-dependent and scale-invariant dynamics, respectively [4–6, 9, 12].

In this work we focus on the scale-dependent early-time and late-time dynamics. We have $\widetilde{\mu} = Bg$ and $\mu = kCv^2$ and hence

$$\frac{\mathrm{d}h}{\mathrm{d}t} = v, \qquad \frac{\mathrm{d}v}{\mathrm{d}t} = Bg - kCv^2. \tag{3.11}$$

The employment of a buoyancy-drag balance to describe Rayleigh–Taylor dynamics has been an ongoing topic for many years [8, 11, 19, 36]. Our momentum model, based on group theory, reconciles with these studies in some limiting cases, and has a number of important advantages, including the direct link of the momentum model to the dynamical system and the governing equations, as follows.

3.3. Link between the dynamical system and the momentum model

We consider RT dynamics within the group theory approach. On the one hand, it is realized in the dynamical system Eqs. (3.6,3.7,3.8,3.9), which is derived from the governing equations (2.1), (2.2) ,(2.3) by employing irreducible representations of the relevant space group. On the other hand, the approach is realized in the momentum model equations (3.10), (3.11), having the same symmetries and scaling transformations as the governing equations. The overarching questions pertain: Can we directly link the two group theory implementations to inclusively handle RT dynamics? Can we precisely derive the buoyancy and drag parameters for the early-time and later-time dynamics? Can we exactly integrate the model equations in the linear and nonlinear regimes? These three questions motivate our study. We answer them here.

4. Results

4.1. Early-time scale-dependent dynamics

The given conditions at initial time t_0 are the initial curvature $\zeta_0 = \zeta(t_0)$ and the initial velocity $v(t_0)$. The latter sets the initial growth rate $v_0 = |v(t_0)|$ and we consider dynamics for $t_0 \gg \tau_G$, the time-scale of the problem. When $t - t_0 \ll \tau_G$, the initial perturbation amplitude is small $|\tau_G k v_0| \ll 1$ and the interface is nearly flat $|\zeta/k| \ll 1$. We associate the curvature ζ with the amplitude, specifically, $kh = -4\zeta/k$. Only first order harmonics need be retained in the moments, that is, $M_0 = 2\Phi_{10}$, $\widetilde{M_0} = 2\widetilde{\Phi}_{10}$ and $M_n = k^n\Phi_{10}$, $\widetilde{M_n} = k^n\widetilde{\Phi}_{10}$, $n \geq 1$ and $M_0 = -\widetilde{M}_0 = -v$. In the early-time linear regime, the buoyancy and the drag parameters are $B = B_l$ and $C = C_l$, where subscript l stands for linear. The equations for the continuity of the normal components of velocity and momentum at the interface, that is equations (3.6) and (3.7), become

$$\frac{\mathrm{d}h}{\mathrm{d}t} = v, \qquad \frac{\mathrm{d}\zeta}{\mathrm{d}t} = -\frac{k^2}{4}v, \qquad \frac{\mathrm{d}v}{\mathrm{d}t} = B_l G t^a - kC_l v^2, \qquad B_l = -4A\frac{\zeta}{k}, \qquad C_l = \frac{A}{2}. \tag{4.1}$$

In the early-time linear regime, the buoyancy parameter is time-dependent, with $B_l \geq 0$ for bubbles and $B_l \leq 0$ for spikes, and the drag parameter is constant, $C_l \geq 0$.

The link between equations (4.1) and the dynamical system equations (3.6), (3.7) is as follows. Equations (3.6) are transformed, recalling that $|\zeta/k| \ll 1$, to

$$\rho_h\left(\frac{\mathrm{d}\zeta}{\mathrm{d}t} - 4M_1\zeta - \frac{1}{2}M_2\right) = 0 \quad \Rightarrow \quad \rho_h\left(-\frac{k^2}{4}\frac{\mathrm{d}h}{\mathrm{d}t} - \frac{k^2}{4}M_0\right) = 0 \quad \Rightarrow \quad \frac{\mathrm{d}h}{\mathrm{d}t} = v,$$

$$\rho_l\left(\frac{\mathrm{d}\zeta}{\mathrm{d}t} - 4\widetilde{M}_1\zeta + \frac{1}{2}\widetilde{M}_2\right) = 0 \quad \Rightarrow \quad \rho_l\left(-\frac{k^2}{4}\frac{\mathrm{d}h}{\mathrm{d}t} + \frac{k^2}{4}\widetilde{M}_0\right) = 0 \quad \Rightarrow \quad \frac{\mathrm{d}h}{\mathrm{d}t} = v \tag{4.2}$$

Similarly, equation (3.7) is transformed to

$$(1+A)\left(-\frac{k}{4}\frac{\mathrm{d}v}{\mathrm{d}t}-\frac{k^2}{8}v^2-\zeta g\right)=(1-A)\left(\frac{k}{4}\frac{\mathrm{d}v}{\mathrm{d}t}-\frac{k^2}{8}v^2-\zeta g\right)$$

$$\Rightarrow\quad -\frac{k}{2}\frac{\mathrm{d}v}{\mathrm{d}t}-\frac{Ak^2}{4}v^2-2A\zeta g=0\quad\Rightarrow\quad \frac{\mathrm{d}v}{\mathrm{d}t}=-\frac{Ak}{2}v^2-\frac{4A}{k}\zeta g\quad\Rightarrow\quad \frac{\mathrm{d}v}{\mathrm{d}t}=\left(-4A\frac{\zeta}{k}\right)g-k\frac{A}{2}v^2 \tag{4.3}$$

Equations (4.2), (4.3) are in full agreement with equations (4.1). The solutions of equation (4.1) are applicable for any sign of $\zeta_0=\zeta(t_0)$ and $v(t_0)/v_0$. They can be combined to give

$$\frac{\mathrm{d}^2\zeta}{\mathrm{d}t^2}-AkGt^a\zeta-\frac{2A}{k}\left(\frac{\mathrm{d}\zeta}{\mathrm{d}t}\right)^2=0. \tag{4.4}$$

For $a>-2$, the dynamics is driven by the acceleration and consequently the relative contributions of the terms is $|AkG\zeta t^a|\gg|(2A/k)(\mathrm{d}\zeta/\mathrm{d}t)^2|$. The transformed system and its solution are

$$\frac{\mathrm{d}^2\zeta}{\mathrm{d}t^2}-Ak^2\zeta Gt^a=0,\qquad v=-\frac{4}{k^2}\frac{\mathrm{d}\zeta}{\mathrm{d}t},\qquad \zeta=-k(kG)^{1/s}\left(C_1\sqrt{t}\;I_p\left(\frac{\sqrt{AkG}}{s}\;t^s\right)+C_2\sqrt{t}\;I_{-p}\left(\frac{\sqrt{AkG}}{s}\;t^s\right)\right). \tag{4.5}$$

where $s=(a+2)/2$, $p=1/(a+2)$, I_p is the modified Bessel function of order p, and C_1 and C_2 are integration constants defined by the initial values $\zeta(t_0)$ and $v(t_0)$.

For $a<-2$, the dynamics is driven by the initial conditions and consequently the relative contributions of the terms is $|AkG\zeta t^a|\ll|(2A/k)(\mathrm{d}\zeta/\mathrm{d}t)^2|$. The transformed system and its solution are

$$\frac{\mathrm{d}^2\zeta}{\mathrm{d}t^2}-\frac{2A}{k}\left(\frac{\mathrm{d}\zeta}{\mathrm{d}t}\right)^2=0,\qquad v=-\frac{4}{k^2}\frac{\mathrm{d}\zeta}{\mathrm{d}t},\qquad \zeta=-\frac{k}{2A}\ln(C_1t+C_2)\qquad v=\frac{2/Ak}{t+C_2/C_1} \tag{4.6}$$

where C_1 and C_2 are integration constants defined by the initial values $\zeta(t_0)$ and $v(t_0)$.

First-order analysis of the very-early-time ($t\sim\ t_0$) dynamics yields

$$\zeta-\zeta_0=-\frac{k}{4}\left(\frac{t-t_0}{\tau_0}\right)\mathrm{sgn}\left[\frac{v(t_0)}{v_0}\right],\qquad v-v_0=-\frac{Av_0}{2}\left(\frac{t-t_0}{\tau_0}\right)\mathrm{sgn}\left[\frac{v(t_0)}{v_0}\right]-\frac{4A}{k}\zeta_0\left(\frac{1}{\tau_g k}\right)\left(\frac{t_0}{\tau_g}\right)^a\left(\frac{t-t_0}{\tau_g}\right). \tag{4.7}$$

which suggests that the positions of bubbles ($\zeta\le0, v\ge0$) and spikes ($\zeta\ge0, v\le0$) are defined by the initial morphology of the interface, with bubbles forming where $\zeta(t_0)<0$ and spikes forming where $\zeta(t_0)>0$. [22]

4.2. Later-time nonlinear dynamics

4.2.1. The buoyancy and the drag parameters

After an initial period of growth of both the curvatures and velocities of the bubbles and spikes their respective curvatures saturate, $\zeta\sim$ constant, and the dynamics transitions to the nonlinear regime. In the late-time nonlinear regime, the buoyancy and drag parameters are $B=B_n$ and $C=C_n$, where the sub-script n stands for nonlinear. Hereafter, we omit the sub-script n for simplicity. In the nonlinear late-time regime, the one-mode approach is insufficient to describe the full set of solutions to the problem. When higher order harmonics are retained in the expressions for the moments, nonlinear asymptotic solutions can be derived.

For $N=1$, the first two harmonics are retained and we arrive at a one-parameter family of solutions, parametrised by the curvature ζ. The far-field, kinematic and momentum requirements when combined yield

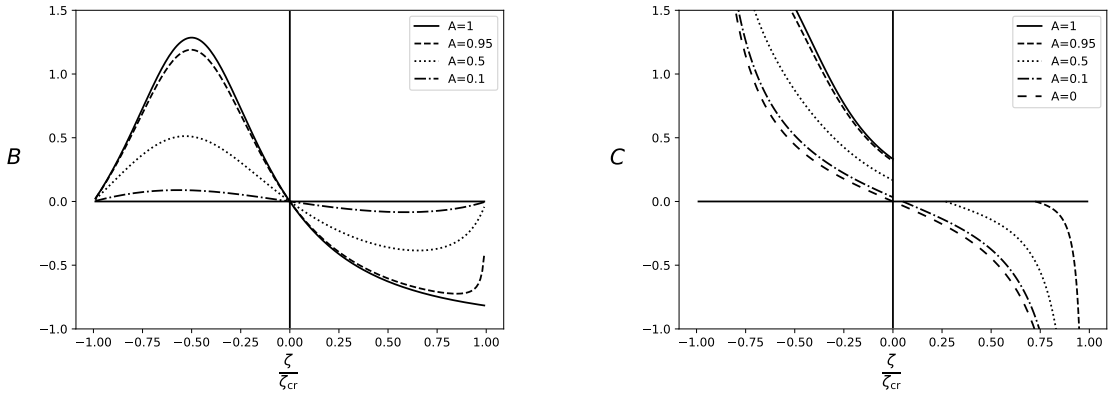

FIGURE 1. Buoyancy and drag parameters in the nonlinear regime as functions of the curvature for various values of the Atwood number.

the single differential equation

$$\frac{\mathrm{d}v}{\mathrm{d}t} = BGt^a - kCv^2, \tag{4.8}$$

where the buoyancy parameter B and drag parameter C depend on the curvature and the Atwood number A. For square symmetry $p4mm$, these quantities are

$$B = \frac{-2A\zeta(9k^2 - 64\zeta^2)}{3k^3 + 10Ak^2\zeta - 128A\zeta^3}, \qquad C = \frac{k^3(9Ak^2 - 48k\zeta + 64A\zeta^2}{(9k^2 - 64\zeta^2)(3k^3 + 10Ak^2\zeta - 128A\zeta^3)}, \tag{4.9}$$

Note that $\zeta < 0$ for bubbles, and $\zeta > 0$ for spikes.

The link between equations (4.8), (4.9) and the dynamical system equations (3.6), (3.7) is demonstrated in the same manner as the link between the early-time equations (4.1) and (3.6). However, the algebra is quite cumbersome and is omitted.

Because bubbles cannot have negative buoyancy and spikes cannot have positive buoyancy, the domain of these functions is $\zeta \in (-\zeta_{\mathrm{cr}}, \zeta_{\mathrm{cr}})$ where $\zeta_{\mathrm{cr}} = \frac{3}{8}k$. In the special case of there being no lower fluid, $A = 1$, the parameters are

$$B = \frac{-2\zeta(3k + 8\zeta)}{16\zeta^2 + 6k\zeta + k^2}, \qquad C = \frac{k^3}{(3k + 8\zeta)(16\zeta^2 + 6k\zeta + k^2)}.$$

Figure 1 shows plots of the buoyancy and drag. Note that $B > 0$ and $C > 0$ for bubbles, and $B < 0$ and $C < 0$ for spikes. For a nearly flat interface,

$$\zeta \approx 0, \qquad B \approx -6A\frac{\zeta}{k}, \qquad C \approx \frac{A}{3} - \frac{2}{9}(8 + 5A^2)\frac{\zeta}{k}.$$

The buoyancy function has extrema B_{ext} at curvatures ζ_{ext}, where the ζ_{ext} satisfy a cubic equation. These are

$$A\zeta_{\mathrm{ext}}^3 + \frac{9}{16}k\zeta_{\mathrm{ext}}^2 - \frac{27}{1024}k^3 = 0, \qquad B_{\mathrm{ext}} = -\frac{256A\zeta_{\mathrm{ext}}^3}{3k^3 + 256A\zeta_{\mathrm{ext}}^3}.$$

The buoyancy function does not have a local minimum when $A = 1$. We note that as $A \to 0$, $\zeta_{\text{ext}} \to \pm k\sqrt{3}/3$.

For any value of the Atwood number, bubble buoyancy reaches a maximum value as the bubble evolves. For very different densities, $A \approx 1$, in the case of bubbles, the maximising curvature and maximum buoyancy are approximately

$$\frac{\zeta_{\max}}{\zeta_{\text{cr}}} \approx -\frac{1}{2} - \frac{1}{18}(1-A), \qquad B_{\max} \approx \frac{9}{7}\left(1 - \frac{32}{21}(1-A)\right).$$

A spike will have unbounded velocity when the drag parameter C is zero. This will occur when $\zeta = \zeta_{\text{sing}}$, where

$$\frac{\zeta_{\text{sing}}}{\zeta_{\text{cr}}} = \frac{1-\sqrt{1-A^2}}{A}. \tag{4.10}$$

Because spikes must have negative values of the drag parameter, spike solutions will only exist for curvatures $\zeta \in (\zeta_{\text{sing}}, \zeta_{\text{cr}})$. The maximising curvature and maximum absolute buoyancy are approximately

$$\frac{\zeta_{\max}}{\zeta_{\text{cr}}} \approx 1 - \frac{\sqrt{6(1-A)}}{3}, \qquad |B_{\max}| \approx \frac{9}{11}\left(1 - \frac{2\sqrt{6(1-A)}}{11}\right).$$

Such spikes will exist for any valid value of the Atwood number A.

The group theory approach allows us to directly derive and quantify the buoyancy parameter and the drag parameter of the momentum model in terms of the tip curvature and the Atwood number in the linear and nonlinear regimes. In the literature, it is often assumed that the parameters B and C are some constant values and are independent of the curvature. However, expressions (4.1) and (4.9) demonstrate that this is far from the case.

4.2.2. The general nonlinear solution

We introduce dimensionless variables to find general nonlinear solutions. When the dynamics is of RM type $a < -2$, or transition type $a = -2$, we choose $\{V = v/v_0,\ T = t/\tau_0\}$. When the dynamics is of RT type $a > -2$, we choose $\{V = v/v_0,\ T = t/\tau_G\}$.

For $a \leq -2$, equation (4.8) becomes

$$\frac{\mathrm{d}V}{\mathrm{d}T} = \alpha_0^2 B T^a - CV^2, \qquad \alpha_0 = \left(\frac{\tau_0}{\tau_G}\right)^{\frac{a+2}{2}} \tag{4.11}$$

For $a > -2$, equation (4.8) becomes

$$\frac{\mathrm{d}V}{\mathrm{d}T} = \frac{B}{\alpha_G} T^a - \alpha_G C V^2, \qquad \alpha_G = \frac{\tau_G}{\tau_0}. \tag{4.12}$$

Equations (4.11), (4.12) are Riccati nonlinear differential equations and can be converted into linear second-order differential equations by making an appropriate change of variable.

For RM dynamics $a < -2$, and RTRM dynamics $a = -2$, let $V = U_T/CU$. For RT dynamics $a > -2$ let $V = U_T/\alpha_G CU$. In each case, the corresponding differential equation is

$$\frac{\mathrm{d}^2 U}{\mathrm{d}T^2} - Q^2 T^a U = 0, \qquad Q = \sqrt{BC} \begin{cases} \alpha_0, & RM:\ a < -2, \\ \sqrt{kG}, & RTRM:\ a = \text{-}2, \\ 1, & RT:\ a > -2. \end{cases} \tag{4.13}$$

Note that the product $BC \geq 0$ for bubbles, which have curvatures $\zeta \in (-\zeta_{\rm cr}, 0)$, and also for spikes, which have curvatures $\zeta \in (\zeta_{\rm sing}, \zeta_{\rm cr})$. For $a \neq -2$, the solution of equation (4.13) is

$$U(T) = C_1\sqrt{T}\ I_p\left(\frac{Q}{s}\ T^s\right) + C_2\sqrt{T}\ I_{-p}\left(\frac{Q}{s}\ T^s\right), \tag{4.14}$$

where $s = (a+2)/2$, $p = 1/(a+2)$, I_p is the modified Bessel function of the first kind of order p, and C_1 and C_2 are integration constants, and for $a = -2$ the solution is

$$U(T) = C_1 T^{(1+\sqrt{1+4Q^2})/2} + C_2 T^{(1-\sqrt{1+4Q^2})/2}. \tag{4.15}$$

The above expressions yield explicit solutions for the velocity $v(t)$ in each case but they are unwieldy. We instead choose to study the constant-curvature behaviour of asymptotic solutions for the equation (4.8).

4.2.3. The power-law asymptotic solutions

In determining asymptotic power-law solutions $v \sim t^b$ of equation (4.8) there are three cases to be considered. When $a < -2$, dominant balance requires that $b = -1$. That is, the acceleration and drag terms dominate the buoyancy term, and the velocity is

$$v_{\rm RM}(t) = \pm\frac{1}{kCt}. \tag{4.16}$$

When $a > -2$, dominant balance requires that $b = a/2$. That is, the drag and buoyancy terms dominate the acceleration term, and the velocity is

$$v_{\rm RT}(t) = \pm\sqrt{\frac{BG}{kC}}t^{\frac{a}{2}}. \tag{4.17}$$

When $a = -2$, dominant balance requires that $b = -1$ and no term is dominated. The velocity is

$$v_{\rm RTRM}(t) = \pm\frac{1+\sqrt{1+4BCkG}}{2kCt}. \tag{4.18}$$

In each case, the positive sign applies for bubbles and the negative sign applies for spikes.

Recall that the Taylor series for the modified Bessel function is

$$I_\nu(z) = \left(\frac{z}{2}\right)^\nu\left(\frac{1}{\Gamma(\nu+1)} + \frac{z^2}{4\Gamma(\nu+2)} + \cdots\right)$$

and that its asymptotic behaviour is

$$I_\nu(z) \ \to\ \frac{\mathrm{e}^z}{\sqrt{2\pi z}}\left(1 - \frac{4\nu^2-1}{8z} + \cdots\right) \quad \text{as} \quad z \to \infty.$$

For $a < -2$, $\nu < 0$ so $T^\nu \to 0$ as $T \to \infty$, and hence the Taylor series is relevant for analysis of the large-time behaviour of RM dynamics. Using this series, we can verify equation (4.16). For $a > -2$, $\nu > 0$ and so $T^\nu \to \infty$ as $T \to \infty$, and hence the asymptotic series is relevant for analysis of the large-time behaviour of RT dynamics. Using this series, we can verify equation (4.17). It is a simple matter to verify equation (4.18) from equation (4.15).

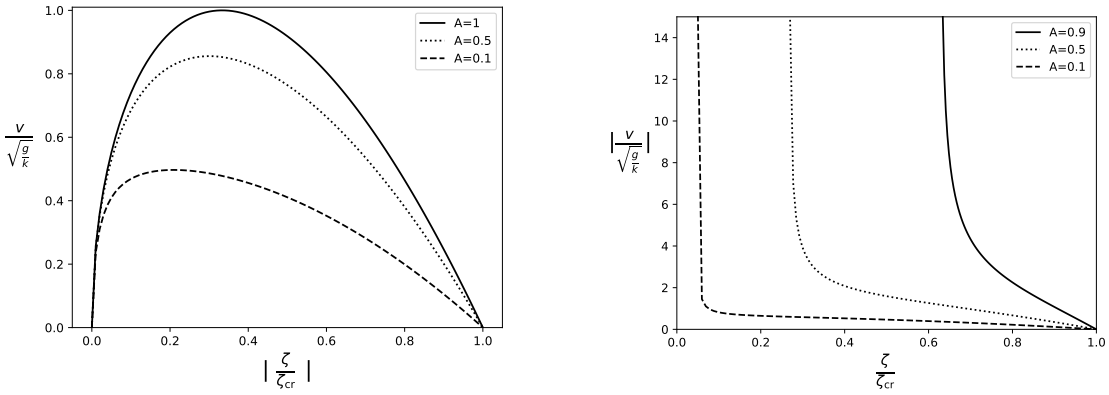

FIGURE 2. Bubble and spike tip velocities as functions of the curvature for various values of the Atwood number in the nonlinear regime.

4.2.4. Nonlinear RT dynamics

As previously mentioned, we are focusing on the square symmetry *p4mm* case. For RT dynamics, $a > -2$, the scaled velocity (Froude number) is

$$\frac{v(t)}{\sqrt{g/k}} = \pm\sqrt{\frac{B}{C}} = \pm\left(\frac{9k^2 - 64\zeta^2}{k^2}\right)\sqrt{\frac{-2Ak\zeta}{64A\zeta^2 - 48k\zeta + 9Ak^2}}. \tag{4.19}$$

The positive sign applies for bubbles and the negative sign applies for spikes. The bubble solutions are valid for curvatures $\zeta \in (-\zeta_{\rm cr}, 0)$, and the spike solutions are valid for curvatures $\zeta \in (\zeta_{\rm sing}, \zeta_{\rm cr})$. Figure 2 shows the bubble and spike tip velocities, respectively, as functions of the curvature. The spike velocity becomes singular at $\zeta = \zeta_{\rm sing}$, as given in equation (4.10).

The bubble velocity achieves its maximum value $v_{\rm max}/\sqrt{g/k}$ at a point $\zeta = \zeta_{\rm vmax}$ which satisfies the quartic equation

$$\zeta_{\rm vmax}^4 - \frac{k}{A}\zeta_{\rm vmax}^3 + \frac{9k^2}{32}\zeta_{\rm vmax}^2 - k^4\left(\frac{3}{16}\right)^3 = 0, \qquad \zeta_{\rm vmax} \in \left(-\frac{k}{8}, 0\right) \tag{4.20}$$

Solving this equation for A and substituting into equation (4.19) gives that the corresponding maximum bubble velocity is

$$v_{\rm max} = 16\sqrt{2}\left|\frac{\zeta_{\rm vmax}}{k}\right|^{\frac{3}{2}}. \tag{4.21}$$

This is a universal relation between the curvature and the maximum velocity. The corresponding buoyancy and drag parameters are, respectively

$$B_{\rm vmax} = \frac{8192\zeta_{\rm vmax}^4}{9k^4 - 320k^2\zeta_{\rm vmax}^2 - 8192\zeta_{\rm vmax}^4}, \qquad C_{\rm vmax} = \frac{-16k^3\zeta_{\rm vmax}}{9k^4 - 320k^2\zeta_{\rm vmax}^2 - 8192\zeta_{\rm vmax}^4}.$$

Note that these are singular at $-(\sqrt{\sqrt{97}-5})/16 \approx -0.138$, However, $\zeta_{\rm vmax}/k$ exceeds -0.125 and hence this is not a concern. If the lower fluid is extremely light then $A \to 1$ and

$$\frac{\zeta_{\rm vmax}}{k} \sim -\frac{1}{8}+\frac{1}{64}(1-A), \qquad \frac{v_{\rm max}}{\sqrt{g/k}} \sim \left|1-\frac{1}{8}(1-A)\right|^{\frac{3}{2}}, \qquad B_{\rm vmax} \sim 1-\frac{13}{8}(1-A), \qquad C_{\rm vmax} \sim 1-\frac{5}{4}(1-A).$$

If the fluid densities are very similar then $A \to 0$ and

$$\frac{\zeta_{\rm vmax}}{k} \sim -\frac{3}{16}A^{\frac{1}{3}}, \qquad \frac{v_{\rm max}}{\sqrt{g/k}} \sim \frac{3\sqrt{3}}{2\sqrt{2}}A^{\frac{1}{2}}, \qquad B_{\rm vmax} \sim \frac{9}{8}A^{\frac{4}{3}}, \qquad C_{\rm vmax} \sim \frac{1}{3}A^{\frac{1}{3}}.$$

4.3. Special solutions for nonlinear RT bubbles

For nonlinear RT bubbles, the family of solutions contains bubbles with distinct values of the velocity, morphology of the interface and Fourier harmonics in the bulk. This multiplicity is due to the presence of the interfacial shear, influencing the curvature and the speed of nonlinear RT bubbles. [5, 18]. Some of the solutions in the continuous family, with the bubble curvature in the interval $\zeta \in (-\zeta_{cr}, 0)$, deserve special attention due to their mathematical and physical aspects.

Beyond the flat bubble, the special solutions include: the critical bubble having maximum curvature magnitude, the convergence limit bubble, the Taylor bubble having constant curvature magnitude, the Layzer-drag bubble having velocity $\sqrt{2A/(1+A)}$ hence dependent on the Atwood number, and the Atwood bubble having the fastest velocity magnitude.

We investigate properties of these special bubbles and determine their buoyancy and drag parameters in the following subsections. We define the dimensionaless curvature as $\hat{\zeta} = \zeta/\zeta_{\rm cr}$ and the dimensionless velocity as $\hat{v} = v/\sqrt{g/k}$, and we use hat overmarks to denote bubble solutions.

4.3.1. The critical bubble

For the critical bubble, the curvature, velocity, and buoyancy and drag coefficients are

$$\left|\hat{\zeta}_{\rm cr}\right| = 1, \qquad \hat{v}_{\rm cr} = 0, \qquad \hat{B}_{\rm cr} = 0, \qquad \hat{C}_{\rm cr} = \infty.$$

This solution is special, since the bubbles in the family of solutions cannot be more curved than the critical bubble. For the critical bubble the velocity is zero.

4.3.2. The convergence-limit bubble

The magnitudes of the Fourier harmonics $|\Phi_{10}(t)|$ and $|\Phi_{20}(t)|$ coincide when $\hat{\zeta} = -5/24$. This defines the convergence-limit bubble solution. For the convergence limit bubble the curvature, velocity, and buoyancy and drag coefficients are

$$\left|\hat{\zeta}_{\rm cl}\right| = \frac{5}{9}, \qquad \hat{v}_{\rm cl} = \frac{14}{9}\sqrt{\frac{30A}{45+53A}}, \qquad \hat{B}_{\rm cl} = \frac{70A}{81-25A}, \qquad \hat{C}_{\rm cl} = \frac{27}{28}\left(\frac{45+53A}{81-25A}\right).$$

For any Atwood number, the convergence-limit bubble is less curved than the critical bubble, and has larger velocity when compared to the critical bubble.

4.3.3. The Taylor bubble

We refer to this bubble as a 'Taylor bubble' since its curvature $\hat{\zeta} = -1/8$ is the same as in the work [16] except for a difference in the wavevector value. For the Taylor bubble, the curvature, velocity, and buoyancy

and drag parameters are

$$\left|\hat{\zeta}_{\mathrm{T}}\right| = \frac{1}{3}, \qquad \hat{v}_{\mathrm{T}} = \sqrt{\frac{8A}{3+5A}}, \qquad \hat{B}_{\mathrm{T}} = \frac{2A}{3-A}, \qquad \hat{C}_{\mathrm{T}} = \frac{5A+3}{4(3-A)}.$$

For any Atwood number, the Taylor bubble is less curved and has larger velocity when compared to the convergence-limit bubble and the critical bubble.

4.3.4. The Layzer-drag bubble

These bubbles have velocity $\hat{v} = \sqrt{2A/(1+A)}$, and consequently the scaled curvature satisfies the quintic equation

$$27(1+A)(\hat{\zeta}_{\mathrm{L}}^5 - 2\hat{\zeta}_{\mathrm{L}}^3) + 8A\hat{\zeta}_{\mathrm{L}}^2 + (11+27A)\hat{\zeta}_{\mathrm{L}} + 8A = 0.$$

The buoyancy and drag parameters are as defined in equation (4.9). We call this solution the Layzer-drag bubble since the Layzer drag model applies this Atwood-number rescaled velocity to the single-mode Layzer first-order approximation at $A = 1$ (see [11, 27]). Experiments and simulations tend to compare well with this rescaling [11, 17, 27].

For fluids with very different densities, letting $A \to 1$ in the solution for the Layzer-drag bubble gives

$$|\hat{\zeta}_{\mathrm{L}}| \sim \frac{1}{3} \mp \frac{\sqrt{6(1-A)}}{18}, \qquad \hat{v}_{\mathrm{L}} \sim 1 - \frac{1-A}{4}, \qquad \hat{B}_{\mathrm{L}} \sim 1 \pm \frac{\sqrt{6(1-A)}}{6}, \qquad \hat{C}_{\mathrm{L}} \sim 1 \pm \frac{\sqrt{6(1-A)}}{6}.$$

For fluids with very similar densities, letting $A \to 0$ in the solution for the Layzer-drag bubble gives

$$|\hat{\zeta}_{\mathrm{L}}| \sim 0.48 - 0.11A, \qquad \hat{v}_{\mathrm{L}} \sim \sqrt{2A}, \qquad \hat{B}_{\mathrm{L}} \sim 0.83A, \qquad \hat{C}_{\mathrm{L}} \sim 0.42 + 0.52A.$$

The Layzer-drag bubble is more curved for fluids with similar densities, $A \to 0$, when compared to fluids with very different densities, $A \to 1$. For fluids with very different densities, $A \to 1$, the values of the curvature, velocity, buoyancy and drag of the Layzer-drag bubble are the same as those of the corresponding quantities of the Taylor bubble. The Layzer-drag bubble is more curved and has smaller velocity when compared to the Taylor bubble.

4.3.5. The Atwood bubble

The fastest member of the family of solutions we refer to as the 'Atwood bubble' to emphasise its dependence on the Atwood number. The curvature which maximises the bubble velocity satisfies equation (4.20). The Atwood bubble is the fastest growing, and hence the physically significant, bubble. The curvature and velocity of the Atwood bubble are

$$\hat{\zeta}_{\mathrm{A}} = \frac{\zeta_{\mathrm{vmax}}}{\zeta_{\mathrm{cr}}}, \qquad \zeta_{\mathrm{vmax}}^4 - \frac{k}{A}\zeta_{\mathrm{vmax}}^3 + \frac{9k^2}{32}\zeta_{\mathrm{vmax}}^2 - k^4\left(\frac{3}{16}\right)^3 = 0, \qquad \hat{v}_{\mathrm{A}} = 16\sqrt{2|\hat{\zeta}_{\mathrm{A}}|^3}$$

and the buoyancy and drag coefficients are as defined in equation (4.9).

For fluids with very different densities, $A \to 1$, the values of the curvature and velocity of the Atwood bubble are the same as those of the corresponding Taylor and Layzer-drag bubbles. For fluids with a finite density ratio, the curvatures relate as $\hat{\zeta}_{\mathrm{A}}/\hat{\zeta}_{\mathrm{cr}} \in (0, 1/3)$, $\hat{\zeta}_{\mathrm{L}}/\hat{\zeta}_{\mathrm{cr}} \in (0, 1/2)$ and $\hat{\zeta}_{\mathrm{A}}/\hat{\zeta}_{\mathrm{T}} \in (0, 1)$. The Atwood bubble is less curved and has larger velocity when compared to the Taylor and Layzer-drag bubbles.

Figure 3 shows plots of the buoyancy and drag parameters as functions of the Atwood number for these special bubbles, and Figure 4 shows plots of the corresponding curvatures and velocities.

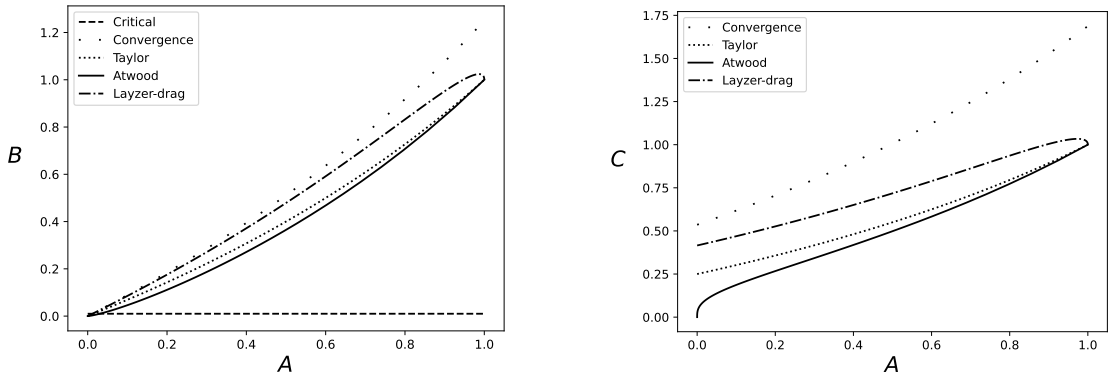

FIGURE 3. Buoyancy and drag as functions of the Atwood number for the special nonlinear RT bubbles. Note that $C \to \infty$ for the critical bubble.

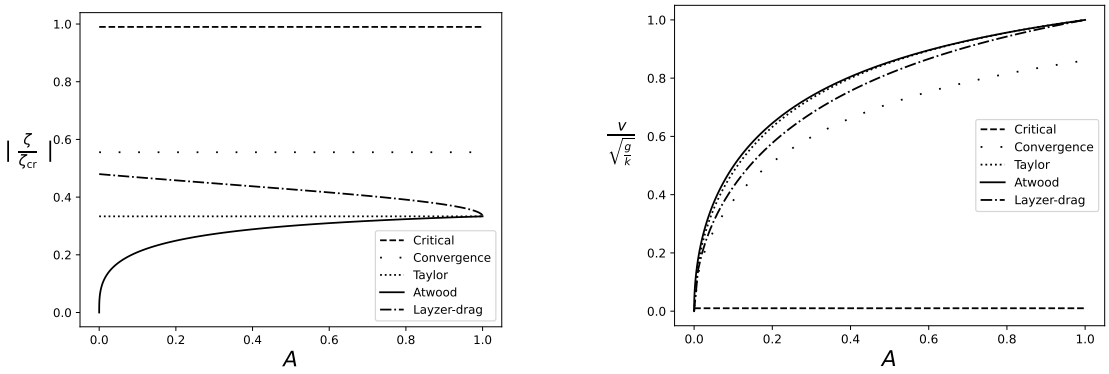

FIGURE 4. Curvature and velocity as functions of the Atwood number for the special nonlinear RT bubbles.

4.4. Special solutions for nonlinear RT spikes

For nonlinear RT spikes, the family of solutions contains spikes with distinct values of the velocity, morphology of the interface and Fourier harmonics in the bulk. This multiplicity is due to the presence of the interfacial shear, influencing the curvature and the speed of the nonlinear RT spikes. [5]. Some of solutions in the continuous family, with the spike curvature in the interval $\zeta \in (0, \zeta_{cr})$, deserve special attention due to their mathematical and physical aspects.

Beyond the flat spike, the special solutions include: the critical spike having maximum curvature magnitude, the convergence limit spike, the Taylor spike having constant curvature magnitude, the Layzer-drag spike having velocity $\sqrt{2A/(1-A)}$ hence dependent on the Atwood number, and the Atwood spike having the fastest velocity magnitude.

We investigate properties of these special spikes and determine their buoyancy and drag parameters in the following sections. We define the dimensionless curvature as $\check{\zeta} = \zeta/\zeta_{\rm cr}$ and the dimensionless velocity as $\check{v} = v/\sqrt{g/k}$, and we use check overmarks to denote spike solutions.

4.4.1. The critical spike

For the critical spike the curvature, velocity, and buoyancy and drag parameters are

$$\check{\zeta}_{\rm cr} = 1, \qquad |\check{v}_{\rm cr}| = 0, \qquad \check{B}_{\rm cr} = 0, \qquad \check{C}_{\rm cr} = -\infty.$$

For the critical spike, the velocity is zero for any density ratio.

4.4.2. The convergence-limit spike

The magnitudes of the Fourier harmonics $|\widetilde{\Phi}_{10}(t)|$ and $|\widetilde{\Phi}_{20}(t)|$ coincide when $\hat{\zeta} = 5/24$. This defines the convergence-limit spike solution. For the convergence-limit spike the curvature, velocity, and buoyancy and drag parameters are

$$\check{\zeta}_{\mathrm{cl}} = \frac{5}{9}, \qquad |\check{v}_{\mathrm{cl}}| = \frac{14}{9}\sqrt{\frac{30A}{45-53A}}, \qquad |\check{B}_{\mathrm{cl}}| = \frac{70A}{25A+81}, \qquad |\check{C}_{\mathrm{cl}}| = \frac{27}{28}\left(\frac{45-53A}{81+25A}\right), \qquad 0 \le A < \frac{45}{53}.$$

For the convergence-limit spike, the velocity has non-positive values which are finite for $0 \le A < 45/53$ and which become singular approaching negative infinity for $A \to 45/53 \approx 0.85$. For any Atwood number, the convergence-limit spike is less curved than the critical spike, $\check{\zeta}_{\mathrm{cl}}/\check{\zeta}_{\mathrm{cr}} = 5/9 \approx 0.56$, and has larger absolute velocity when compared to the critical spike.

4.4.3. The Taylor spike

We refer to this spike as a 'Taylor spike' since its curvature magnitude is the same as in the work [16] of Davis & Taylor except for a difference in the wavevector value. For the Taylor spike the curvature, velocity, and buoyancy and drag parameters are

$$\check{\zeta}_{\mathrm{T}} = \frac{1}{3}, \qquad |\check{v}_{\mathrm{T}}| = \sqrt{\frac{8A}{3-5A}}, \qquad |\check{B}_{\mathrm{T}}| = \frac{2A}{3+A}, \qquad |\check{C}_{\mathrm{T}}| = \frac{3-5A}{4(3+A)}, \qquad 0 \le A < \frac{3}{5}.$$

For the Taylor spike, the velocity has non-positive values which are finite for $0 < A < 3/5$ and which become singular approaching negative infinity for $A \to 3/5 = 0.6$. For any Atwood number, the Taylor spike is less curved than the convergent-limit spike and the critical spike, $\check{\zeta}_{\mathrm{T}}/\check{\zeta}_{\mathrm{cr}} = 1/3$ and $\check{\zeta}_{\mathrm{T}}/\check{\zeta}_{\mathrm{cl}} = 3/5$. The Taylor spike also has larger absolute velocity.

4.4.4. The Layzer-drag spike

This family of spikes has velocity $|\check{v}| = \sqrt{\frac{2A}{1-A}}$, and consequently the scaled curvature satisfies the quintic equation

$$27(1-A)(\check{\zeta}_{\mathrm{L}}^5 - 2\check{\zeta}_{\mathrm{L}}^3) + 8A\check{\zeta}_{\mathrm{L}}^2 + (11-27A)\check{\zeta}_{\mathrm{L}} + 8A = 0.$$

The buoyancy and drag parameters are as defined in equation (4.9). We call this solution the Layzer-drag spike since the Layzer drag model applies this Atwood-number rescaled velocity to the single-mode Layzer first-order approximation at $A = 1$ (see [11, 27]).

For fluids with very different densities, letting $A \to 1$ in the solution for the Layzer-drag spike gives

$$\check{\zeta}_{\mathrm{L}} \sim 1 - \sqrt{2(1-A)}, \qquad |\check{v}_{\mathrm{L}}| \sim \sqrt{\frac{2}{1-A}}, \qquad |\check{B}_{\mathrm{L}}| \sim \frac{9}{11}\left(1 - \frac{4}{11}\sqrt{2(1-A)}\right), \qquad |\check{C}_{\mathrm{L}}| \sim \frac{9}{22}(1-A).$$

For fluids with very similar densities, letting $A \to 0$ in the solution for the Layzer-drag spike gives

$$\check{\zeta}_{\mathrm{L}} \sim 0.48 + 0.11A, \qquad |\check{v}_{\mathrm{L}}| \sim \sqrt{2A}, \qquad |\check{B}_{\mathrm{L}}| \sim 0.83A, \qquad |\check{C}_{\mathrm{L}}| \sim 0.42 - 0.52A.$$

The Layzer-drag spike is more curved for fluids with very different densities $A \to 1$ than for fluids with very similar densities $A \to 0$. The Layzer-drag spike is less curved than the critical spike and is more curved than

the Taylor spike, the ratios being $\check{\zeta}_{\rm L}/\check{\zeta}_{\rm cr} \in (\sqrt{9-4\sqrt{3}}/3, 1)$ and $\check{\zeta}_{\rm L}/\check{\zeta}_{\rm T} \in (\sqrt{9-4\sqrt{3}}, 3)$. The Layzer-drag spike has smaller absolute velocity when compared to that of the Taylor spike.

The curvatures of the Layzer-drag spike and the convergence-limit spike equal one another at $A = 235/451 \approx 0.52$, and for larger values of the Atwood number the Layzer-drag spike solutions may not converge.

For fluids with very similar densities $A \to 0$, the magnitude of the curvature of the Layzer-drag spike is the same as that for the Layzer-drag bubble. The magnitude of the velocity of the Layzer-drag spike differs from that of the Layzer-drag bubble: The velocity magnitude of the spike approaches infinity for $A \to 1$, whereas the velocity magnitude of the bubble is finite for any A.

4.4.5. The Atwood spike

The fastest spike is when the drag coefficient $C = 0$. We refer to this spike as the 'Atwood spike' to emphasise its dependence on the Atwood number. It is the fastest growing, and hence the physically significant, spike. For the Atwood spike, the curvature is regular, $\check{\zeta} \to \check{\zeta}_{\rm A}$, whereas the velocity is singular, with $|\check{v}_{\rm A}| \to \infty$ for any Atwood number.

For fluids with very different densities, $A \to 1$, the solution for the Atwood spike is:

$$\check{\zeta}_{\rm A} \sim 1 - \sqrt{2(1-A)}, \qquad\qquad |\check{B}_{\rm A}| \sim \frac{9}{11}\left(1 - \frac{4}{11}\sqrt{2(1-A)}\right).$$

For fluids with very similar densities, $A \to 0$, the solution for the Atwood spike is:

$$\check{\zeta}_{\rm A} \sim \frac{1}{2}A, \qquad\qquad |\check{B}_{\rm A}| \sim \frac{9}{8}A^2.$$

The Atwood spike is less curved than the Layzer-drag spike for $A \in [0, 1)$ and has the same curvature as the Layzer-drag spike $\check{\zeta}_{\rm A}/\check{\zeta}_{\rm L} = 1$ at $A = 1$. The Atwood spike attains the same curvature as the critical spike at $A = 1$, the same curvature as the Taylor spike at $A = 3/5$, and the same curvature as the convergence-limit spike at $A = 45/53 \approx 0.85$. For $A > 45/53$ the Atwood spike solutions may not converge.

The properties of the curvature and velocity of the Atwood spike differ dramatically from those of the Atwood bubble: For any density ratio, the magnitude of the velocity of the Atwood spike is singular whereas the magnitude of the velocity of the Atwood bubble is regular and finite. While the magnitudes of the curvature of the Atwood spike and the Atwood bubble are both finite, the Atwood spike is more curved when compared to the Atwood bubble for fluids with very different densities $A \to 1$ and less curved when compared to the Atwood bubble for fluids with very similar densities $A \to 0$.

Figure 5 shows plots of the buoyancy and drag as functions of the Atwood number for these special spikes, and Figure 6 shows plots of the corresponding curvatures and velocities.

4.5. Interfacial dynamics

RT dynamics is essentially interfacial, with intense fluid motion near the interface and with effectively no fluid motion away from the interface. The formation of RT bubble/spike is determined by the initial conditions, with the bubble (spike) moving up (down) and being concave down (up). The dynamics is single-scale in the early-time (linear) regime and multi-scale in the nonlinear regime, where it is set by the spatial period and amplitude of the structural array of bubbles and spikes.

Figure 7 shows the qualitative velocity fields of the Taylor bubble and Taylor spike in the inertial reference frame in the (x, z)-plane for Atwood number $A = 1/2$. Shear-driven vortical structures may appear at the interface due to the discontinuity of the tangential component of velocity. Near the tip of the bubble the vortical structures 'rotate' from the heavy to the light fluid. This velocity pattern is observed in experiments and simulations, demonstrating excellent qualitative agreement with our results [9, 19, 25, 29, 30, 34, 37].

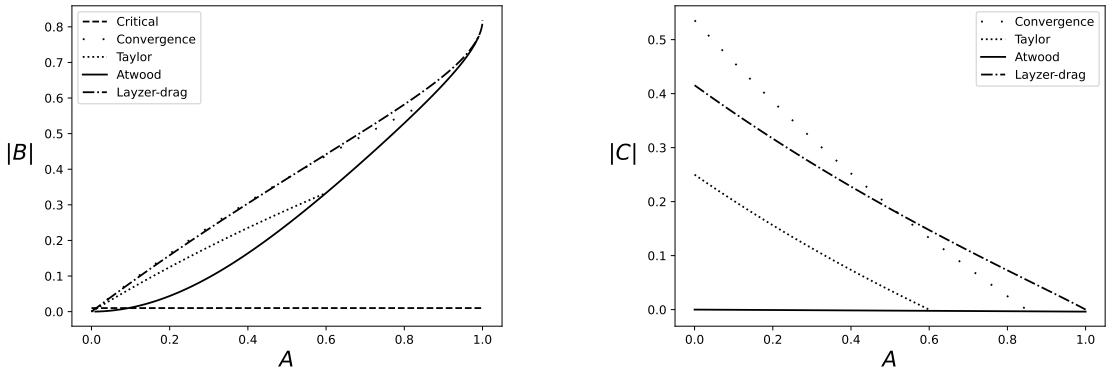

FIGURE 5. Buoyancy and drag as functions of the Atwood number for the special nonlinear RT spikes. Note that $|C| \to \infty$ for the critical spike.

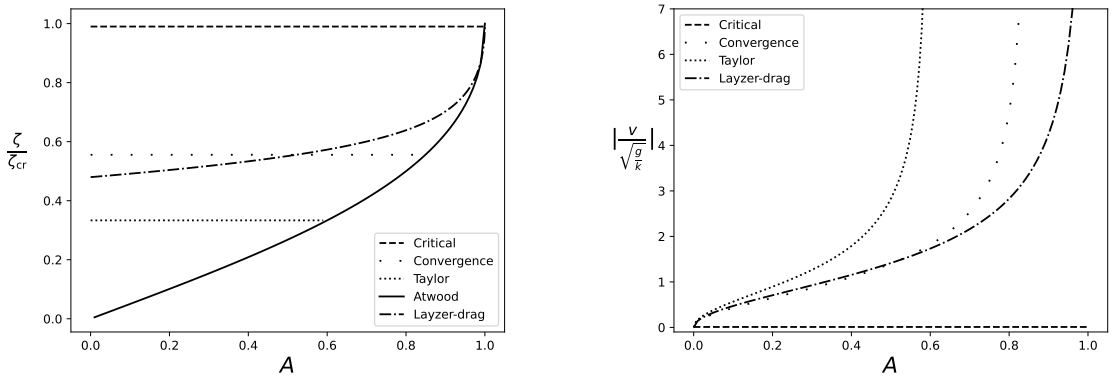

FIGURE 6. Curvature and velocity as functions of the Atwood number for the special nonlinear RT spikes. Note that $|v/\sqrt{g/k}| \to \infty$ for the Atwood spike in the nonlinear regime.

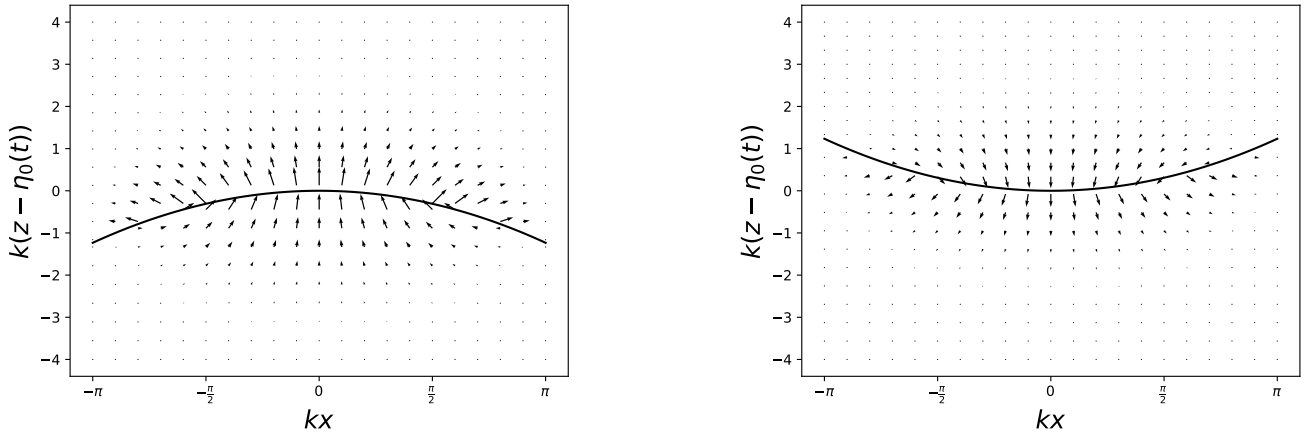

FIGURE 7. Qualitative velocity fields of the nonlinear Taylor bubble and the nonlinear Taylor spike for $A = 1/2$ in the (x, z)-plane in the laboratory reference frame.

5. Discussion

We have investigated RT dynamics using the group theory approach by directly linking the two group theory implementations - the dynamical system based on space groups and the momentum model based on symmetries and scaling transformations. The dynamics is driven by the specific balance of the rates of momentum gain and loss, and the buoyancy and drag parameters are distinct in different regimes.

We have precisely derived expressions for the buoyancy and drag parameters from the conservation laws and the boundary conditions for a three-dimensional spatially extended periodic flow with square symmetry in the plane normal to the acceleration. We have exactly integrated the model equations and found their solutions in both the early-time and later-time regimes.

For the nonlinear RT dynamics, we have studied a number of special bubbles and spikes, including those with largest curvature values, convergence-limit solutions, Taylor solutions with constant curvature magnitudes, Layzer-drag solutions, and the Atwood (fastest) solutions. We defined the Layzer-drag solutions by using a velocity re-scaling of RT bubbles/spikes with which observations tend to compare well. For RT bubbles, the Atwood (fastest) solution corresponds to the curved bubble with regular velocity. For RT spikes, the Atwood (fastest) solution corresponds to the curved spike with singular velocity.

Our analysis captures the physics of the early-time linear and the late-time nonlinear RT dynamics. Our theory can be extended to higher orders, including spatial expansion of the governing equations and the Fourier harmonics of the heavy and light fluids, leading to minor quantitative corrections, similarly to previous work [1, 7]. Our analysis can also be extended to other symmetries and dimensionalities, including two-dimensional flows and three-dimensional flows with, for example, hexagonal, rhombic and rectangular symmetries in the plane normal to the acceleration direction [5, 9]. This permits a systematic investigation of early-time and constant-curvature RT dynamics. Our results are consistent with existing studies [9, 10, 15, 21, 25, 28, 33] and elaborate new benchmarks for future experiments and simulations.

References

[1] S. Abarzhi, Steady state flows in Rayleigh–Taylor instability. *Phys. Rev. Lett.* **81** (1998) 337–340.

[2] S. Abarzhi, Low-symmetric bubbles in Rayleigh–Taylor instability. *Phys. Fluids* **13** (2001) 2182–2189.

[3] S. Abarzhi, Review on nonlinear coherent dynamics of unstable fluid interface: conservation laws and group theory. *Physica Scripta* **T132** (2008) 014012.

[4] S. Abarzhi, On fundamentals of Rayleigh–Taylor turbulent mixing. *Europhys. Lett.* **91** (2010) 35000.

[5] S. Abarzhi, Review of theoretical modeling approaches of Rayleigh–Taylor instabilities and turbulent mixing. *Phil. Trans. R. Soc. A* **368** (2010) 1809–1828.

[6] S. Abarzhi, A. Gorobets and K. Sreenivasan, Turbulent mixing in immiscible, miscible and stratified media. *Phys. Fluids* **17** (2005) 081705.

[7] S. Abarzhi, K. Nishihara and R. Rosner, Multiscale character of the nonlinear coherent dynamics in the Rayleigh–Taylor instability. *Phys. Rev. E* **73** (2006) 036310.

[8] S. Abarzhi and R. Rosner, Comparative study of approaches for modeling Rayleigh–Taylor turbulent mixing. *Physica Scripta* **T142** (2010) 014012.

[9] S.I. Abarzhi, A. Bhowmick, A. Naveh, A. Pandian, N. Swisher, R. Stellingwerf and W. Arnett, Supernova, nuclear synthesis, fluid instabilities and interfacial mixing. *Proc. Natl. Acad. Sci. U.S.A.* (2018) 201714502.

[10] B. Akula, P., Suchandra, M. Mikhaeil and D. Ranjan, Dynamics of unstably stratified free shear flows: an experimental investigation of coupled Kelvin–Helmholtz and Rayleigh–Taylor instability. *J. Fluid Mech.* **816** (2017) 619–660.

[11] U. Alon, J. Hecht, D. Offer and D. Shvarts, Power laws and similarity of Rayleigh–Taylor and Richtmyer–Meshkov mixing fronts at all densities. *Phys. Rev. Lett.* **74** (1995) 534.

[12] S. Anisimov, R. Drake, S. Gauthier, E. Meshkov and S. Abarzhi, What is certain and what is not so certain in our knowledge of Rayleigh–Taylor mixing? *Phil. Trans. R. Soc. A* **371** (2013) 20130266.

[13] D. Arnett, Supernovae and Nucleosynthesis: An Investigation of the History of Matter, from the Big Bang to the Present. Princeton University Press (1996).

[14] M. Buehler, H. Tang, A. van Duin and W. Goddard, Threshold crack speed controls dynamical fracture of silicon single crystals. *Phys. Rev. Lett.* **99** (2007) 165502.

[15] S. Chandrasekhar, Hydrodynamic and Hydromagnetic Stability. Oxford University Press (1961).

[16] R. Davies and G. Taylor, The mechanics of large bubbles rising through extended liquids and through liquids in tubes. *Proc. R. Soc. A* **200** (1950) 375–390.

[17] G. Dimonte, et al. A comparative study of the turbulent Rayleigh–Taylor instability using high-resolution three-dimensional numerical simulations: the alpha-group collaboration. *Phys. Fluids* **16** (2004) 1668–1693.

[18] P. Garabedian, On steady-state bubbles generated by Taylor instability. *Proc. R. Soc. A* **241** (1957) 423.
[19] J. Glimm, D. Sharp, T., Kaman and H. Lim, New directions for Rayleigh–Taylor mixing. *Phil. Trans. R. Soc. A* **371** (2013) 20120183.
[20] S. Haan, Point design targets, specifications, and requirements for the 2010 ignition campaign on the national ignition facility. *Phys. Plasmas* **18** (2011) 051001.
[21] D.L. Hill and S.I. Abarzhi, On the Rayleigh–Taylor unstable dynamics of 3D interfacial coherent structures with time-dependent acceleration. *AIP Adv.* **9** (2019) 075012.
[22] D.L. Hill and S.I. Abarzhi, On the dynamics of Richtmyer–Meshkov bubbles in unstable 3d interfacial coherent structures with time-dependent acceleration. *Phys. Fluids* **32** (2020) 062107.
[23] D.L. Hill and S.I. Abarzhi, On Rayleigh–Taylor and Richtmyer–Meshkov dynamics with inverse quadratic power-law acceleration. *Front. Appl. Math. Stat.* **7** (2022) 735526.
[24] D.L. Hill, A.K. Bhowmich, D.V. Ilyin and S.I. Abarzhi, Group theory analysis of early-time scale-dependent dynamics of the Rayleigh–Taylor instability with time varying acceleration. *Phys. Rev. Fluids* **4** (2019) 063905.
[25] K. Kadau, J. Barber, T. Germann, B. Holian and B. Alder, Atomistic methods in fluid simulation. *Phil. Trans. R. Soc. A* **368** (2010) 1547.
[26] L. Landau and E. Lifshitz, Course of Theoretical Physics. Pergamon Press, New York (1987).
[27] D. Layzer, On the instability of superposed fluids in a gravitational field. *Astrophys. J.* **122** (1955) 1.
[28] S. Lugomer, The time scale for the transition to turbulence in a high Reynolds number, accelerated flow. *Laser Part. Beams* **34** (2016) 123–135.
[29] E. Meshkov, Instability of the interface of two gases accelerated by a shock. *Sov. Fluid Dyn.* **4** (1969) 101–104.
[30] E. Meshkov, Some peculiar features of hydrodynamic instability development. *Phil. Trans. R. Soc. A* **371** (2013) 20120288.
[31] A. Pandiani, N. Swisher and S. Abarzhi, Deterministic and stochastic dynamics of Rayleigh–Taylor mixing with a power-law time-dependent acceleration. *Physica Scripta* **92** (2017) 014002.
[32] L. Rayleigh, Investigations of the character of the equilibrium of an incompressible heavy fluid of variable density. *Proc. London Math. Soc.* **14** (1883) 170–177.
[33] B. Remington, et al. Rayleigh–Taylor instabilities in high-energy density settings on the national ignition facility. *Proc. Natl. Acad. Sci. U.S.A.* (2018) 201717236.
[34] H. Robey, Y. Zhou, A. Buckingham, P. Keiter, B. Remington and R. Drake, The time scale for the transition to turbulence in a high Reynolds number, accelerated flow. *Phys. Plasmas* **10** (2003) 614.
[35] N. Swisher, et al. Rayleigh–Taylor mixing in supernova experiments. *Phys. Plasmas* **22** (2015) 102707.
[36] B. Thornber, et al. Late-time growth rate, mixing, and anisotropy in the multimode narrowband Richtmyer–Meshkov instability. *Phys. Fluids* **29** (2017) 105107.
[37] D. Youngs, The density ratio dependence of self-similar Rayleigh–Taylor mixing. *Phil. Trans. R. Soc. A* **371** (2013) 20120173.
[38] Y. Zeldovich and Y. Raizer, Physics of Shock Waves and High-temperature Hydrodynamic Phenomena. Dover, New York (2002).